 

# *Accounts*

## Infrared Spectroscopic Study of Water–Aromatic Hydrocarbon Mixtures at High Temperatures and Pressures.

**Seiya Furutaka,* Hitomi Kondo, and Shun-ichi Ikawa***

Division of Chemistry, Graduate School of Science, Hokkaido University, Sapporo, 060-0810

(Received April 9, 2001)

This paper reviews recent infrared studies on water–aromatic hydrocarbon mixtures. It mainly deals with infrared absorption of HDO in hydrocarbons measured as a function of temperature and pressure in the 373–648 K and 100–350 bar ranges, respectively. The intensity ratio of a hydrogen-bonded OH band to a hydrogen-bond-free OH band increases with increasing temperature. This fact indicates that the rate of increase in water solubility in the hydrocarbons is large enough to surmount the entropy effect which is unfavorable to water–water association. A good correlation between the peak frequency of the hydrogen-bond-free band and ionization potential of solvent hydrocarbons suggests that the concept of π-hydrogen bonding between water and aromatic hydrocarbons is useful even at high temperatures and pressures. At higher temperatures, the two OH bands mentioned above merge into a single band, which suggests that a water molecule rotates rather freely even in a hydrogen-bonded water cluster at high enough temperature. Water concentration and density of a hydrocarbon-rich phase are estimated from infrared intensities. Both of them show remarkable pressure dependence near an extended line of the three-phase coexistence curve in the phase diagram. This behavior should be characteristics of fluid mixtures near the critical region.

It is well known that water and hydrocarbons are almost immiscible or only poorly miscible with each other at ambient condition, and the hydrocarbons are usually described as hydrophobic. However, their mutual solubilities increase significantly with increasing temperature under pressure, and finally, they become completely miscible at any mixing ratio. Water and benzene, for example, form a homogeneous mixture at temperatures and pressures above 570 K and 200 bar, respectively.[1–4] Such a wide range variation of the solubility as a function of temperature and pressure will be useful to a study of intermolecular interaction of water with hydrocarbons. This interaction is generally weak and has not been thoroughly studied because most of the experimental data available are limited to the very dilute solutions. Nevertheless, the water–hydrocarbon interaction is concerned with a wide variety of naturally occurring phenomena. It is particularly important to studies of formation and stabilization of the native structure of proteins in solution, where hydration of the hydrophobic side chains and water trapped in the hydrophobic cavities are thought to play important roles.[5–7] Furthermore, elucidation of the water–hydrocarbon interaction will be useful to assessment and suitable treatment of contamination of water by hydrocarbons from petrochemical plants, factories, laboratories, etc.[8,9]

### 1. Background

The mixtures of water and hydrocarbons at high temperatures and pressures have also been given much attention in a wide range of industrial situations. Characterization of the mixtures is indispensable to designs, operations, and maintenance of equipment or plants for oil refineries, coal gasification and liquefaction plants, gas industry and petrochemical industry.[10–13] It is likely that oil reservoirs have been formed by geothermal processes involving high temperature water–hydrocarbon mixtures.[12] Physicochemical properties of the mixtures are also important for designing an environment-protecting technology where hydrothermal reactions are applied to destruction of toxic waste chemicals.[14–18] Even benzene is completely oxidized in supercritical water with oxygen at temperatures higher than 850 K and 250 bar.[19] To understand and design those industrial processes, thermodynamic properties of the mixtures are of essential importance and have been widely studied.[10–12,20–22] Among others, phase behavior is the most basic property and has been extensively studied for mixtures of water with simple hydrocarbons, such as methane, hexane, and benzene.[10,11,23–29]

**1.1. Phase Behavior of Water–Hydrocarbon Mixtures.** Figure 1 shows a pressure–temperature phase diagram for water–benzene mixtures, which is drawn by using literature data.[4,11] The 3-phase line indicates a liquid–liquid–gas coexistence equilibrium curve with a critical end point at 542.6 K and 94.6 bar.[23] At pressures above this line, the gas phase disappears and two liquid phases, namely water-rich and benzene-rich liquid phases, coexist. The thick solid line connecting the 3-phase end point and the critical point of neat benzene (562.2

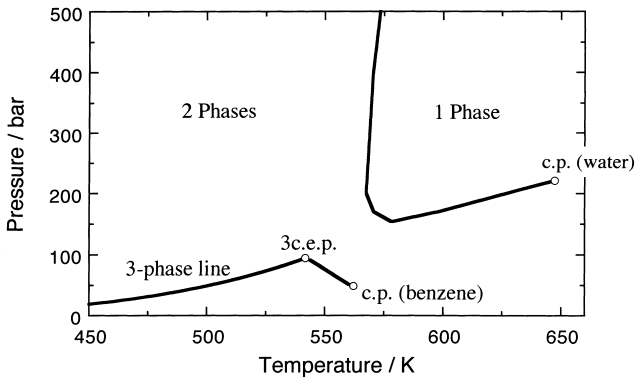


Fig. 1. Pressure-temperature phase diagram for water–benzene mixtures.
Thick solid line: one-phase critical curve and liquid–liquid–gas three-phase equilibrium curve; c.p.: critical point; 3c.e.p.: three-phase critical end point.

K and 49.0 bar)[30] is a critical curve indicating the highest temperature at which all three phases coexist: above this curve the benzene-rich liquid phase disappears. The critical curve around the homogeneous one-phase region ends at the critical point of neat water (647.3 K and 220.5 bar).[30] A phase diagram with these features is classified as type III following Scott and van Konynenburg.[31] Most of water–hydrocarbon mixtures are included in the type III mixtures, while the phase diagrams of mixtures in general are classified into six principal features, type I to type VI. The critical points of water and aromatic hydrocarbons studied in the present paper are given in Table 1.

In addition to the phase diagrams, thermodynamic properties such as heat of mixing, excess molar enthalpy and dielectric coefficients have been reported for water–hydrocarbon mixtures at high temperatures and pressures.[12,21,32] Nevertheless, mutual solubility data are scarce. Even for the water–benzene mixture, which has been most extensively studied so far, the solubility data have been limited at the three-phase equilibrium pressures,[11,33] and at a few other pressures at higher temperatures[2,32] to our knowledge. This is due to difficulty in measurements of the mutual solubiltites at high temperatures and pressures. Usually a small amount of mixtures equilibrated in a high temperature-pressure vessel is sampled and transferred to analytical instruments such as gas chromatographs and Karl Fisher titration instruments for composition analysis. The transferring of a sample without disturbing equilibrium and/or without composition change is difficult, particularly at high temperature and high pressure.[33] In addition, density measurements at high temperature and pressure add another difficulty, and the solubility data are usually given by molar fractions. It is really difficult to directly measure the density of each phase in the coexistence region of two phases. However, the densities of components in the equilibrated phases are important to understand the physicochemical properties of the mixtures on the basis of the intermolecular interactions.

Table 1. Critical Points of Hydrocarbons and Water

| Pure substances[a] | | |
|---|---|---|
| | $T_c$/K | $P_c$/bar |
| Benzene | 562.2 | 49.0 |
| Toluene | 591.7 | 41.1 |
| Ethylbenzene | 617.1 | 36.1 |
| *o*-Xylene | 630.2 | 37.3 |
| *m*-Xylene | 617.0 | 35.5 |
| Mesitylene | 637.3 | 32.0 |
| Water ($H_2O$) | 647.3 | 220.5 |
| Water ($D_2O$) | 643.9 | 216.7 |
| **Mixtures** | **(Three-phase critical end point)** | |
| | $T_{cep}$/K | $P_{cep}$/K |
| Water–Benzene[b] | 542.6 | 94.6 |
| Water–Toluene[b] | 558.1 | 100.94 |
| Water–Ethylbenzene[c] | 568.1 | 106.8 |

a) Ref. 30, b) Ref. 23, c) Ref. 25.

**1.2. Vibrational Spectroscopy of Water in Hydrocarbons.** A solution to the experimental problems mentioned above can be obtained by spectroscopic in situ measurements. Vibrational spectroscopy is particularly useful for measuring water in hydrocarbons. The OH stretching band of water is strong enough not to be masked by absorption of most of solvent hydrocarbons. Moreover, the peak frequency, the integrated intensity, and profile of the band is sensitive to local environment and hydrogen bonding of the water molecules. Therefore, the vibrational spectroscopy is one of the most powerful tools for investigating molecular level structure of fluid mixtures. Actually, infrared spectroscopy has been often applied to the problem of whether or not water aggregates exist in non-polar solvents.[34–38] It is now commonly accepted that water is primarily monomeric in benzene and its alkyl derivatives and in saturated hydrocarbons. It has been suggested, however, that a few percent of dissolved water in benzene and carbon tetrachloride exist in a dimeric form.[35,37] The vibrational spectroscopy has also been used in the study of dynamics of water molecules in hydrocarbons.[38–40] The band profile provides detailed information particularly about reorientational motion of solute molecules.

In spite of those advantages, only a few papers have been reported for vibrational spectroscopic measurements of the water–hydrocarbon mixtures at high temperatures and pressures. Tassaing[41] studied vibrational spectra of water confined in benzene in the temperature range 298–578 K and at a constant pressure of 160 bar. From analyses of the peak positions, the band intensities and band profiles, the author has indicated that water forms a weak π-hydrogen bond with benzene. In addition, it has been shown that hydrogen-bonded water dimers appear at the expense of the water–benzene complex as the concentration of water increases in the mixture. Pironon et al.[42] studied the solubility of water in hydrocarbons trapped in petroleum inclusions at temperatures in the range of 298–573 K, which covers the conditions of natural petroleum reservoirs, by Raman and FT-IR measurements. They have obtained bulk homogenization temperatures of the petroleum inclusions from a measurement that the liquid water band disappears due to dissolution of water into the oil phase. Recently, we have studied water–hydrocarbon mixtures at temperatures up to 648 K and pressures up to 350 bar by infrared spectroscopy.[43–46] Results of these studies and some newly obtained results are re-

viewed in the following.

## 2. Experimental Methods

**2.1. Experimental Setup.** The experimental setup we have used is schematically shown in Fig. 2. The high-pressure cell is a custom-made cell machined by SITEC-Sieber Engineering, Switzerland. The cell body is made of nickel-base superalloy, Nimonic 80A, which is useful for applications requiring high strength and corrosion resistance up to 1100 K. The maximum operating temperature and pressure of the cell are 673 K and 1000 bar, respectively. The windows of the cell are colorless sapphire cylinders of 10 mm diameter and 8 mm thickness, which are transparent at frequencies higher than 2000 $cm^{-1}$. These windows are pressed against optically polished flat surfaces of window plugs for the pressure seal by Poulter's unsupported area principle.[47] The effective aperture for the optical transmission is 6 mm and the optical path length of a sample is fixed at 1 mm. The cell is heated by a flexible electric heating tape wound around the cell and the sample temperature is measured with a chromel-alumel thermocouple. Pressure of the sample is measured with a pressure transducer of a semiconductor strain gauge (PDCR 960, Druck, England) and a pressure indicator (DPI 261, Druck). The cell is set in a sample compartment of a BOMEM DA3 Fourier-transform spectrometer, which is equipped with a $CaF_2$ beamsplitter and a mercury–cadmium–telluride detector.

**2.2. Infrared Measurements.** Water specimens were mixtures of $H_2O$ and $D_2O$ with a ratio of 1 : 20 or 1 : 30. Then the ratios of the isotopic species, $H_2O$, HDO, and $D_2O$ are estimated to be 1 : 40 : 400 or 1 : 60 : 900. Therefore, the contribution of $H_2O$ to the infrared OH stretching absorption can be approximately neglected and the observed OH bands are assigned only to HDO to a good approximation. Using HDO mixtures instead of neat $H_2O$ and $D_2O$ has a few advantages. First, we can avoid the complication of spectra due to overlap of the symmetric and antisymmetric stretching bands, and then we can attribute temperature- and pressure-dependent changes of band profiles directly to changes in equilibrium of water–water association or dynamics of molecules. The next advantage of measuring HDO in these mixtures is to reduce the OH absorption band intensity. When a neat $H_2O$ specimen is used, the absorption intensity becomes too strong to measure at higher temperatures and pressures, due to a great increase in water solubility in hydrocarbons. Another important advantage is that $D_2O$-saturated hydrocarbons can be used as references for obtaining absorbance of HDO, when hydrocarbons have absorption bands in the OH stretching region. This is the case for water–benzene mixtures. Benzene exhibits two combination bands in the 3600–3700 $cm^{-1}$ region, which change in shape by interaction with dissolved water particularly at temperatures higher than 530 K where water solubility in benzene becomes significantly large. To obtain OH absorption bands of HDO in benzene, therefore, we have to use $D_2O$-saturated benzene as the reference to completely cancel the absorption of benzene. It would be difficult to find a suitable reference when a neat $H_2O$ specimen is used. Other hydrocarbons used in the present study, on the other hand, have no appreciable absorption in the OH stretching region, and neat hydrocarbons can be used as the reference. In addition to the OH stretching region, we have measured spectra in the 4500–4800 $cm^{-1}$ region for water–hydrocarbon mixtures and neat hydrocarbons. Absorption in this region is assigned to a few combination bands characteristic of a phenyl group, and its integrated intensity is used for estimates of hydrocarbon concentrations in the hydrocarbon-rich phase.

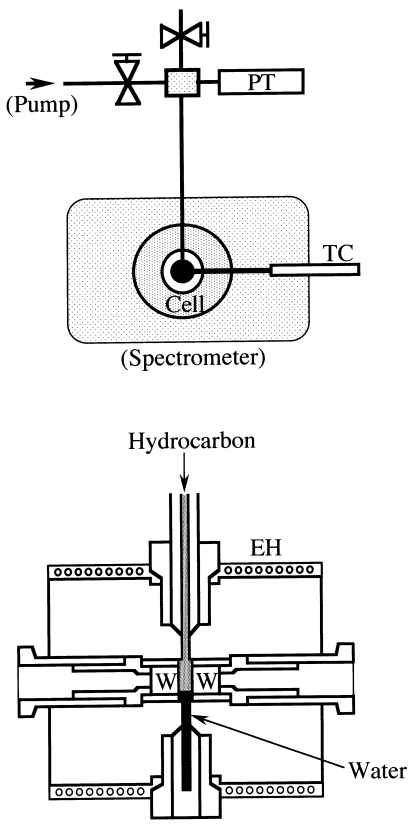


Fig. 2. Schematics of the experimental setup (upper) and the high pressure-temperature cell (lower). PT: pressure transducer, TC: thermocouple, EH: electric heating tape, W: sapphire windows.

Spectroscopic grade hydrocarbons, benzene, toluene, ethylbenzene, *o*- and *m*-xylenes, and mesitylene from Nacalei Tesque (Japan) and deuterium oxide (99.9% D) from CEA (France) were used as received. A small amount of the water specimen is put in the cell, and then compressed liquid hydrocarbons are transmitted into the cell with a syringe pump for liquid chromatography (L-6000, Hitachi, Japan). The level of the water–hydrocarbon interface was adjusted to slightly below the optical axis to measure the hydrocarbon-rich phase. The spectral measurements were performed with 2 $cm^{-1}$ resolution at sample temperatures in the 373–648 K (±0.5 K) range and pressures in the 100–350 bar (±1 bar) range. Each of the experimental temperature–pressure points was attained at a slow enough rate, and the phase equilibrium of the mixture was confirmed by a spectrum that was unchanged for at least an hour. The sample was not agitated to avoid emulsification. The resulting spectra of the OH stretching region are given by absorption coefficients,

$$\alpha(\nu) = \frac{1}{x_{\mathrm{HDO}} \cdot l} \ln \frac{I_0(\nu)}{I(\nu)} \tag{1}$$

where $x_{\mathrm{HDO}}$ denotes the molar fraction of HDO in the water specimen, $l = 0.1$ cm is the sample thickness, and $I_0(\nu)$ and $I(\nu)$ are the transmission intensities at $\nu$ $cm^{-1}$ of the reference and the sample, respectively, measured at the same temperature and pressure.

## 3. Infrared Absorption of Water in Hydrocarbons at High Temperatures and Pressures

The frequencies, profile, and intensities of the vibrational spectra tell about various molecular level features of the fluid mixtures, such as the nature of the intermolecular interaction, dynamics of molecules, molar concentration, and the densities. How these properties vary with temperature and pressure is important for physicochemical characterization of the mixtures. The spectral features of the water–hydrocarbon mixtures significantly depend on the temperature and pressure, as will be seen later. For convenience, description of the spectra in the following is separated into two ranges of the temperatures: lower and higher than the temperature of the three-phase critical end point.

**3.1. At Temperatures below the Three-Phase Critical Temperature.** Figure 3 shows examples of spectra for water–benzene mixtures at a few temperatures at 100 bar. The absorption intensity increases greatly with increasing temperature, indicating increase in concentration of water in benzene. Furthermore, the band profile exhibits remarkable change. At 373 K, only a single peak at about 3640 $cm^{-1}$ is seen. However, a shoulder at about 3580 $cm^{-1}$ grows remarkably with increasing temperature. These temperature-dependent spectral changes have been commonly observed for all the water–hydrocarbon mixtures studied in the present paper. However, the peak position varies depending on solvent hydrocarbons as will be shown later. The 3640 $cm^{-1}$ peak is assigned to a HDO monomer and the 3580 $cm^{-1}$ band to hydrogen-bonded OH of a dimeric species of $D_2O\cdots HDO$[43] from comparison with frequencies observed in the gas phase and in low-temperature matrices,[48–52] which are summarized in Table 2.

**(1) Monomer–Dimer Equilibrium.** In order to separate the absorption into the hydrogen-bond-free and the hydrogen-bonded bands, we have resolved the observed spectra into a few components with Lorentzian and Gaussian profiles. Figure 4 shows an example of least-squares fitting of the band of the water–benzene mixture at 473 K and 100 bar. A band at about 3910 $cm^{-1}$ is assigned to a combination band of $D_2O$, which is observed owing to using neat benzene as reference, and is excluded in the following discussion. The broad band with the center at about 3800 $cm^{-1}$ is assigned to a vibration-rotation transition of the monomeric species, which corresponds to those found in low-temperature matrices.[50,53]

To discuss monomer-dimer equilibium, we have estimated the integrated intensities,

$$A_{OH} = \int_{band} \alpha(\nu) d\nu \qquad (2)$$

of the components bands. Intensities of the hydrogen-bond-free band are obtained by a sum of the 3640 $cm^{-1}$ and the 3800 $cm^{-1}$ bands, and those for the hydrogen-bonded bands by a

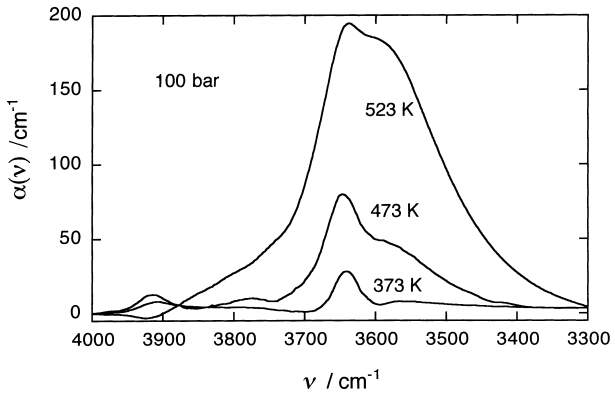


Fig. 3. Infrared OH stretching absorption of HDO in benzene at a few temperatures at 100 bar.

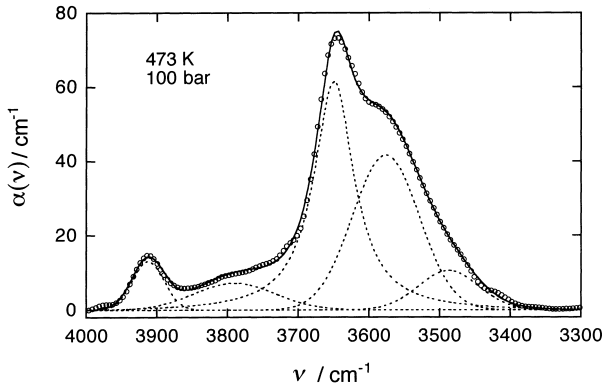


Fig. 4. Decomposition of the infrared OH absorption of HDO in benzene at 473 K and 100 bar. Open circle: observed; solid line: calculated total; dotted line: calculated components.

Table 2. Observed Wavenumbers of $\nu_3$(OH) Stretching of HDO in various states.*

| Solvent | | $\nu^{free}/cm^{-1}$ | $\nu^{bonded}/cm^{-1}$ | |
|---|---|---|---|---|
| Benzene | (373 K) | 3641.0 | | |
| | (473 K) | 3648.6 | 3570 (−79) | |
| | (523 K) | 3652.0 | 3590 (−62) | |
| | | | $\nu^{dimer}/cm^{-1}$ | $\nu^{trimer}/cm^{-1}$ |
| Gas | | 3707.47[a] | 3616 (−91)[b] | 3529 (−178)[b] |
| Ne | (matrix) | 3699.0[c] | | |
| Ar | (matrix) | 3688[d] | 3590 (−98)[b] | 3520 (−168)[b] |
| $N_2$ | (matrix) | 3681.6[e] | 3562 (−120)[e] | |

*Figures in parentheses are wavenumber shifts from $\nu^{free}$.
a) Ref. 48, b) Ref. 49, c) Ref. 50, d) Ref. 51, e) Ref. 52.

sum of the two lower-frequency components. Strictly speaking, we should have taken account of the lower frequency counterpart of the 3800 $cm^{-1}$ band. However, it is masked by the hydrogen-bonded bands and is difficult to separate from them. Neglect of the lower frequency counterpart will not change the following discussion.

The resulting intensities of the OH absorption bands are plotted against temperature in Fig. 5. The total intensity increases by an order of magnitude as the temperature increases from 373 K to 523 K, indicating an increase in the water concentration since the intensity should be proportional to the water concentration. In addition, it is found that the intensity ratio of the hydrogen-bonded band to the hydrogen-bond-free band increases with the increasing temperature. This fact indicates that the relative ratio of the dimeric species to the monomeric species increases with increasing temperature. In general, the increase in temperature has two mutually opposite effects on the equilibrium. The increase in solubility of water in benzene is favorable to the hydrogen-bonded species owing to the law of mass action. On the other hand, an entropy effect favorable to the hydrogen-bond-free species increases also with increasing temperature.

Assuming a monomer-dimer equilibrium,

$$2W \longleftrightarrow W_2 \tag{3}$$

the equilibrium constant is given by

$$K = \frac{d}{2C(1-d)^2} \tag{4}$$

where $C$ is the total concentration of water and $d$ indicates the degree for the dimer formation. The population ratio of the dimer to the monomer is given by

$$r = \frac{d}{1-d} \tag{5}$$

From Eqs. 4 and 5, $r$ is obtained as

$$r = \frac{1}{2}(\sqrt{8CK+1}-1) \tag{6}$$

The first derivative of $r$ with respect to temperature $T$ is given by

$$\frac{dr}{dT} = \frac{2}{\sqrt{8CK+1}}\frac{d}{dT}(CK) \tag{7}$$

Using the experimental result $dr/dT > 0$, we obtain

$$\frac{1}{C}\frac{dC}{dT} > -\frac{1}{K}\frac{dK}{dT} \tag{8}$$

This relationship indicates that the rate of increase in the water concentration is larger than the rate of decrease in the equilibrium constant. This is the condition for the effect of solubility increase to be superior to the entropy effect, and is found to be fulfilled in all the water–hydrocarbon mixtures measured in the present study.

Figure 6 shows the effect of pressure on the OH band at constant temperatures, 473 K and 523 K. In contrast to the remarkable temperature effect on the band intensity mentioned above, the effect of pressure is only seen at around the peak of the hydrogen-bond-free band. The total band intensity is approximately independent of pressure, indicating constant water concentration in the 100 to 350 bar range. However, it is worthwhile to note that the relative intensity of the hydrogen-bond-free peak to the shoulder assigned to the hydrogen-bonded OH increases with increasing pressure. This fact suggests that the water–water hydrogen bond is destabilized a little as the increasing pressure strengthens the water–benzene interaction.

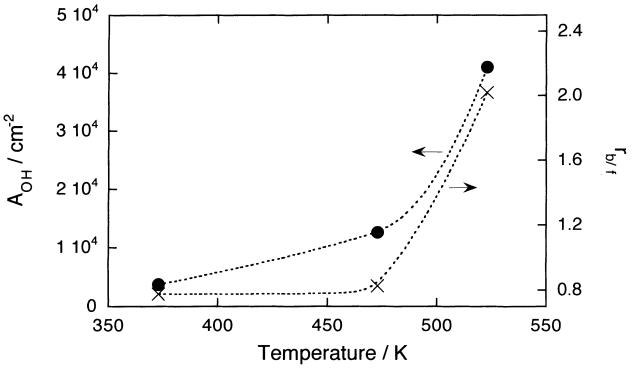


Fig. 5. Effect of temperature on the integrated intensities of the OH stretching absorption (left ordinate) and intensity ratios (right ordinate) of the hydrogen-bonded band to the hydrogen-bond-free band of HDO in benzene.

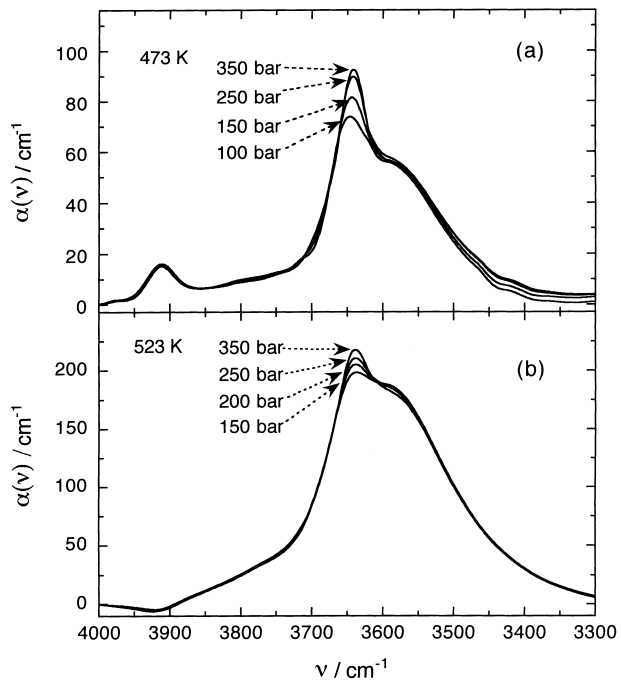


Fig. 6. Infrared OH stretching absorption of HDO in benzene at 473 K (a) and 523 K (b) at a few pressures. (Reproduced from Ref. 45 with permission. Copyright (2000) American Institute of Physics).

**(2) π-Hydrogen Bonding.** Next, we consider the varia-

tion of peak frequencies of the hydrogen-bond-free peak with alkyl substituents of the phenyl ring. As mentioned before, the band profile of HDO is about the same for all the water–hydrocarbon mixtures studied, but the peak frequencies are dependent on the alkyl substituents and occur in the order: benzene > toluene > ethylbenzene > *o*-xylene–*m*-xylene > mesitylene. This fact gives a clue to the nature of the intermolecular interaction between water and the hydrocarbons. Another intriguing point is that the peak frequency of the monomeric HDO in benzene at 473 K and 100 bar, 3648.6 $cm^{-1}$, is near to that of a water–benzene complex, 3649 $cm^{-1}$, which was observed for a jet-cooled cluster with resonant ion-dip infrared spectroscopy.[54] This agreement suggests that the monomeric water in benzene at high temperature and pressure undergoes a similar interaction to that in the low-temperature complex, in which water forms a hydrogen bond with benzene, with one of its hydrogen atoms pointing toward the midpoint of the benzene ring,[54–56] as illustrated in Fig. 7. In this configuration, the π-electron of the benzene ring is thought to act as a hydrogen-bond acceptor and to form a π-hydrogen bond with water. Therefore, the present experimental results mentioned above may also be explained by the π-hydrogen-bonding interaction. The strength as the hydrogen-bond acceptor will be related to the ionization potential of the hydrocarbons, which is a measure of electron-release tendency. Actually, the above-mentioned order of the peak frequencies is exactly the same as the order of ionization potentials of the aromatic hydrocarbons.

A useful model for the π-hydrogen-bonding between water and aromatic hydrocarbons has been proposed by Ratajczak and Orville–Thomas[57] on the basis of Mulliken's charge transfer theory.[58] They derived the following relationship between the OH stretching peak frequency, $\nu_p$, and the vertical ionization potential, $I_D$, of the electron-donor molecule (aromatic hydrocarbon in the present case):

$$(\Delta\nu)^{-1} = \frac{a}{\beta_0^2}(I_D - E_A - C) \tag{9}$$

where $\Delta\nu = \nu_r - \nu_p$ is the peak frequency shift from a certain reference frequency, $\nu_r$, which is free from the charge transfer interaction, $a$ is constant for structurally similar hydrogen-bonded complexes, $E_A$ is the vertical electron affinity of the electron-acceptor molecule (water in the present case), $C$ denotes the difference in stabilization energy between the excited (charge-transfer) state and the ground state, and $\beta_0$ is a resonance integral between the donor and acceptor orbitals. For convenience, Eq. 9 is rewritten as,

$$(\Delta\nu)^{-1} = m \cdot I_D + n \tag{10}$$

where

$$m = a\beta_0^{-2} \tag{11}$$

$$n = -a\beta_0^{-2}(E_A + C) = -m(E_A + C) \tag{12}$$

Thus, a linear relationship is expected between $(\Delta\nu)^{-1}$ and $I_D$. As the reference frequency, $\nu_r$, we adopt the frequency of HDO dissolved in hexane measured at 473 K and 100 bar, $\nu_r$ = 3679.3 $cm^{-1}$.[59] This frequency may involve a similar interaction to that in aromatic hydrocarbons except for the charge transfer interaction. The resulting values of $(\Delta\nu)^{-1}$ are plotted against $I_D$ in Fig. 8. The plots are obviously linear, as expected above, and indicate that the interaction between water and aromatic hydrocarbons in the mixtures at high-temperatures and pressures can be described as the π-hydrogen bonding as that in their complexes observed at the very low-temperatures. The stabilization energy of the charge transfer state is approximately given by the Coulomb energy of the ion pair and, in general, much larger than that of the ground state.[60] Therefore, $C$ can be approximated by the net attractive energy of the ion pair, $C = q^2/(4\pi\varepsilon_0 r)$, where $q = 1.602 \times 10^{-19}$ C is the elementary electric charge and $\varepsilon_0 = 8.854 \times 10^{-12}$ F $m^{-1}$ is the electric permittivity of vacuum. Consequently, the distance $r$ between water and benzene is given by the following relationship

$$r = \frac{q^2}{4\pi\varepsilon_0 - [(n/m) - E_A]} \tag{13}$$

The value of $n/m$ is estimated as $-6.4 \pm 0.1$ from eV the slope and the intercept of the plots in Fig. 8, and the electron affinity of water has been reported as $E_A$ = 1.2 eV.[61] Using these values, $r$ is estimated to be 2.8 ± 0.1 Å, which is comparable to

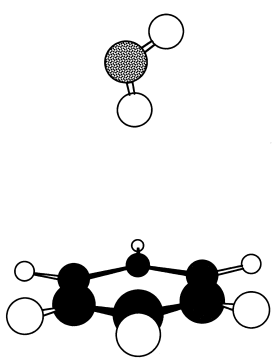

Fig. 7. Configuration of a water–benzene complex.

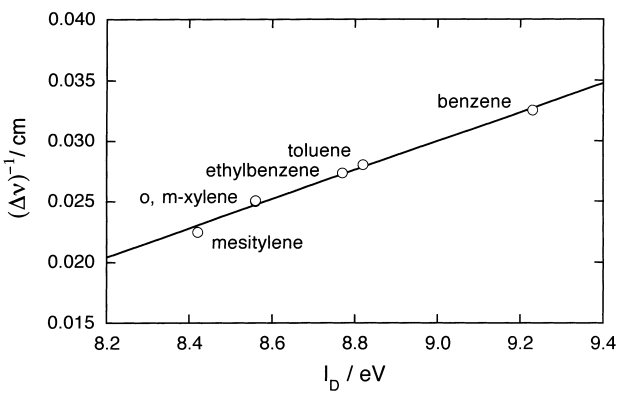


Fig. 8. Plots of the frequency shifts of the OH stretching of HDO against ionization potentials of solvent aromatic hydrocarbons at 473 K and 100 bar.

those previously reported for the low-temperature complex. In the MP-2 optimized structure,[62] the distance from the center-of-mass of benzene to the π-bonded hydrogen atom is 2.302 Å, and that from the water center-of-mass to the benzene center-of-mass is 3.210 Å, which is in fair agreement with the experimental value of 3.347 Å determined from jet cooled microwave spectra.[56] Although the distance $r$ in Eq. 13 is difficult to concretely define, it seems reasonable that the $r$ value is in the middle of the two explicitly defined distances mentioned above, because the electron accepting orbital of water is considered to be an anti-bonding orbital of the OH bond. Therefore, the present experimental result of $r$ gives another support to describing the water–benzene interaction in the high-temperature-pressure mixtures with the concept of π-hydrogen bonding.

**3.2. At Temperatures above the Three-Phase Critical Temperature.** Spectral behavior of the water–hydrocarbon mixtures at temperatures higher than the three-phase critical point is significantly different from that at the lower temperatures. Figure 9 shows examples of the spectra observed for the water–benzene mixture at some temperatures at constant pressure 300 bar. In the temperature range from 523 to 573 K, the absorption increases with increasing temperature similarly to the temperature-dependent increase in the lower temperature range shown in Fig. 3. However, with further rising of the temperature, the absorption decreases rather steeply. The same phenomena have been observed for the water–toluene and water–ethylbenzene mixtures, although the temperatures of the maximum absorption shift to the higher temperature values, as shown in Fig. 10. These facts indicate that the water concentration in the hydrocarbon-rich phase of the water–aromatic hydrocarbon mixtures passes a turning point as the temperature increases at constant pressure. Positions of the turning points are in the vicinity of the critical curves as will be shown later.

**(1) Dynamical Feature of the Water–Water Hydrogen Bond.** It is intriguing that the band shapes at higher temperatures are more symmetric and structure-less as compared with those at lower temperatures, as seen in Figs. 9 and 10. The change in the band shapes is more clearly shown in Fig. 11, in which each spectrum is normalized at the peak maximum. At the lower temperatures, the hydrogen-bond-free and hydrogen-bonded bands can be separately recognized. On the other hand, the absorption at the higher temperatures seems to be difficult to decompose. On the contrary, the distinction between the hydrogen-bond-free and hydrogen-bonded bands seems to be meaningless. It is rather likely that the two bands merge into a single band at the higher temperatures, at which a water molecule would acquire enough rotational energy to cleave a hydrogen bond within a hydrogen-bonded cluster. The hydrogen bond energy of water, about 20 kJ mol$^{-1}$, is much larger than the thermal energy at the present temperature

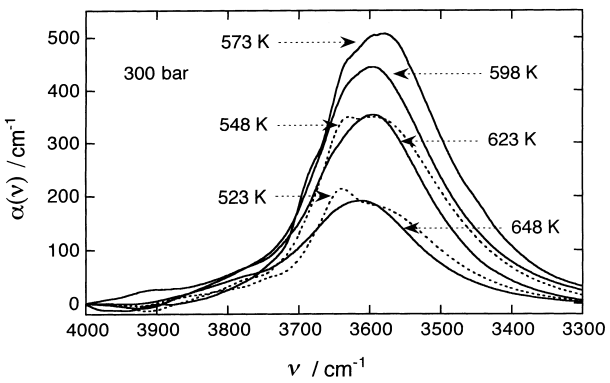


Fig. 9. Effect of temperature on the infrared absorption of HDO in benzene at 300 bar.

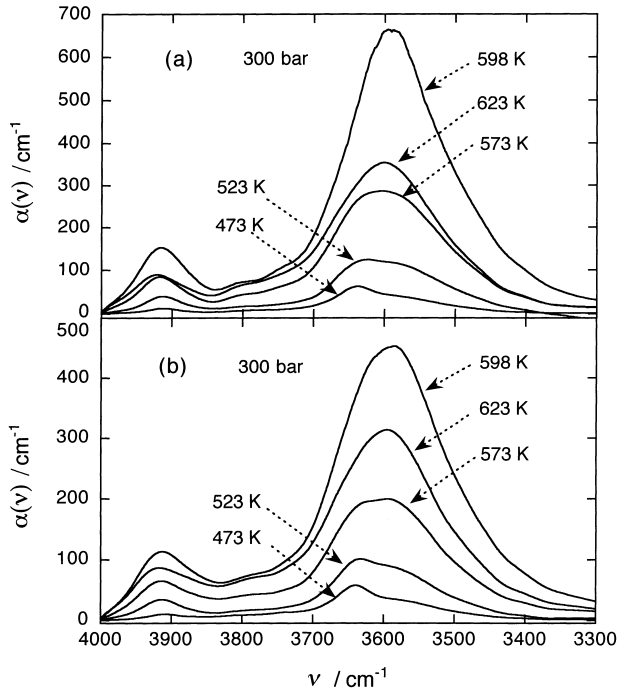


Fig. 10. Effect of temperature on the infrared absorption of HDO in toluene (a) and ethylbenzene (b) at 300 bar.

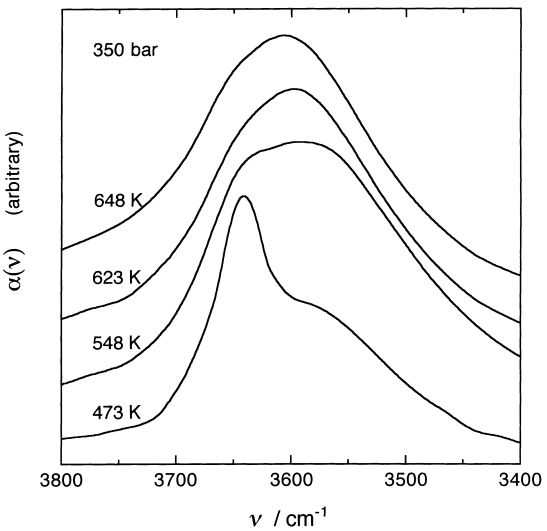


Fig. 11. Effect of temperature on the band profile of the OH absorption of HDO in benzene at 350 bar. (Reproduced from Ref. 45 with permission. Copyright (2000) American Institute of Physics).

range, 5.4 kJ mol$^{-1}$ at 648 K. In such conditions, a hydrogen-bonded cluster will continue to exist for a certain period which is long enough in the time scale of infrared measurements. On the other hand, the energy barrier for molecular rotation within the hydrogen-bonded cluster may be comparable to the thermal energy. The energy barrier for a hydrogen-bonded water dimer, for example, is estimated to be about 6 kJ mol$^{-1}$ from ab initio calculations by Matsuoka et al.,[63] assuming that the bifurcated configuration is a transition state, as illustrated in Fig. 12. At high enough temperature, therefore, the OH bond of the HDO molecule changes back and forth between the hydrogen-bonded (G) and hydrogen-bond-free (G′) states with high enough frequency. Consequently the two bands merge into a single band by the same principle as that for the well-known phenomenon called signal coalescence due to chemical exchange in the NMR spectra. The low limit of the exchange rate to yield the band coalescence can be estimated from frequency difference between the two bands. The rate constant at the coalescence temperature is given by

$$k_c = \pi c \Delta\nu / \sqrt{2}, \tag{14}$$

where $c$ is the speed of light and $\Delta\nu$ denotes the frequency difference between the two bands. Using the wave numbers 3648 and 3580 cm$^{-1}$, $k_c$ is estimated to be $5 \times 10^{12}$ s$^{-1}$, and a rotational lifetime of the hydrogen bonds in the water cluster is given as $2 \times 10^{-13}$ s.

**(2) Temperature–Pressure Dependence of the OH Band Intensity.** Effect of pressure on the spectra is shown in Fig. 13. In contrast to the very small pressure effect at the lower temperatures seen in Fig. 6, the absorption intensity as a measure of water concentration increases by an order of magnitude as the pressure increases from 100 to 350 bar. Since the absorption at the higher temperatures is difficult to decompose into component bands, we have obtained the integrated intensities of the whole OH absorption for a quantitative discussion. The integrated intensities are summarized in Fig. 14 for the water–benzene mixture. It is clearly shown that the intensities at 473 and 523 K are almost independent of pressure. On the contrary, at the higher temperatures, the intensities increase remarkably with increasing pressure and then reach or seem to reach constant values at the higher pressures. The rate of the initial increase is the steepest at 548 K and gradually reduces as the temperature rises. These phenomena can be properly understood by referring to a phase diagram which includes positions of the typical experimental points as shown in Fig. 15

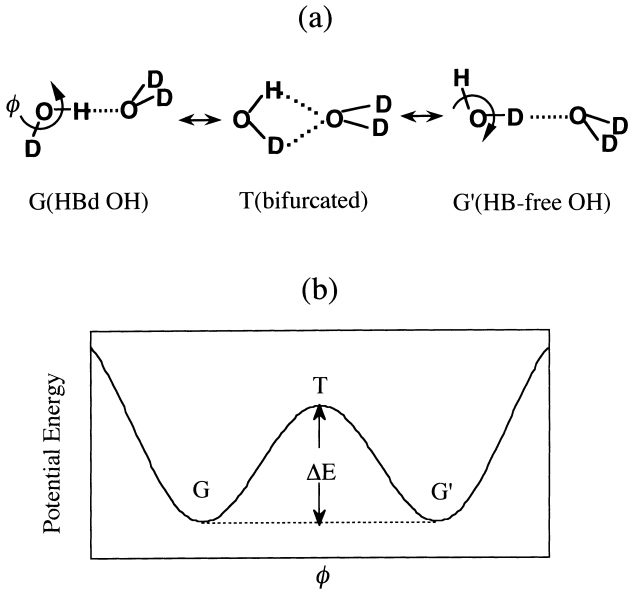


Fig. 12. Schematics of an exchange mechanism between the hydrogen-bonded and hydrogen-bond-free states of an OH group within a water dimer (a) and a potential energy curve for the rotational jump (b).

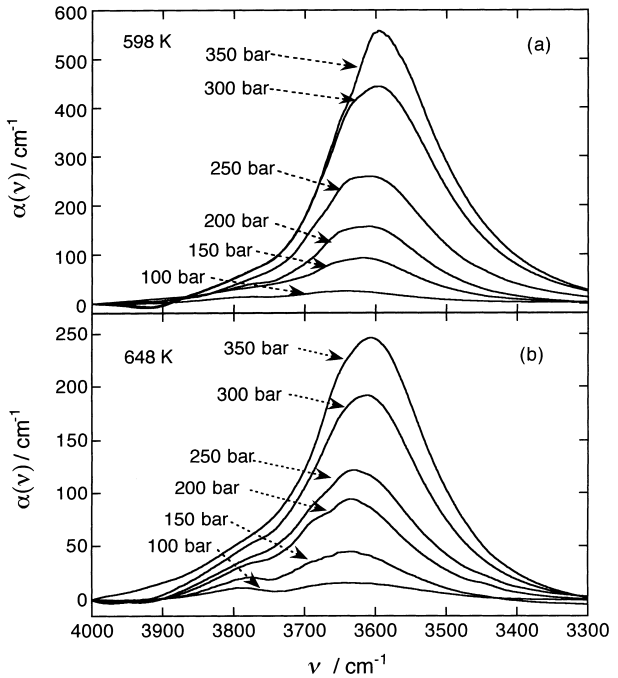


Fig. 13. Infrared absorption of HDO in benzene at 598 K (a) and 648 K (b) at some pressures.

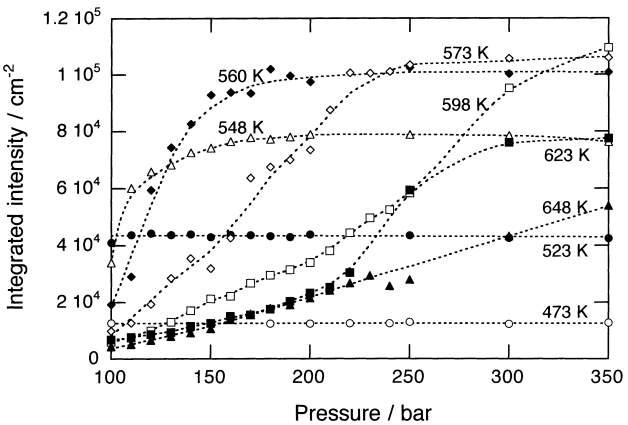


Fig. 14. Integrated intensities of HDO in benzene plotted against pressure.
(Reproduced from Ref. 45 with permission. Copyright (2000) American Institute of Physics).

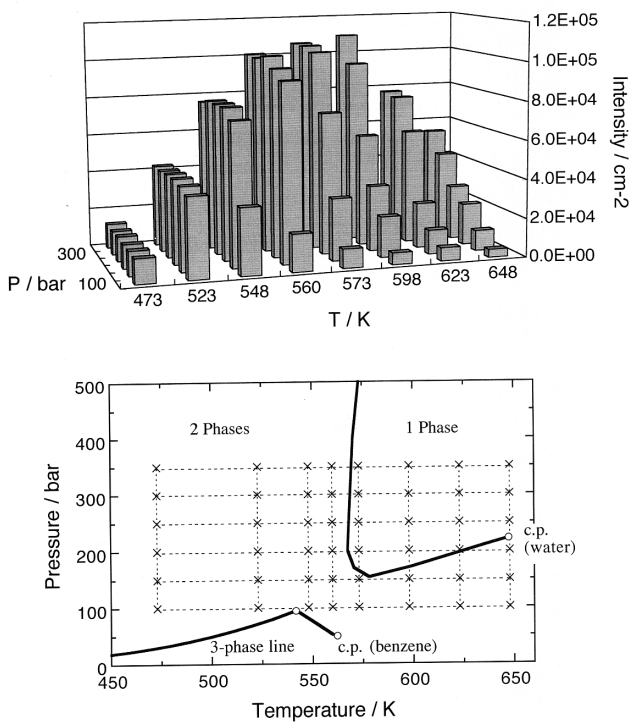


Fig. 15. Infrared intensity map for HDO in the benzene-rich phase (upper) and the typical experimental points indicated in the phase diagram (lower).

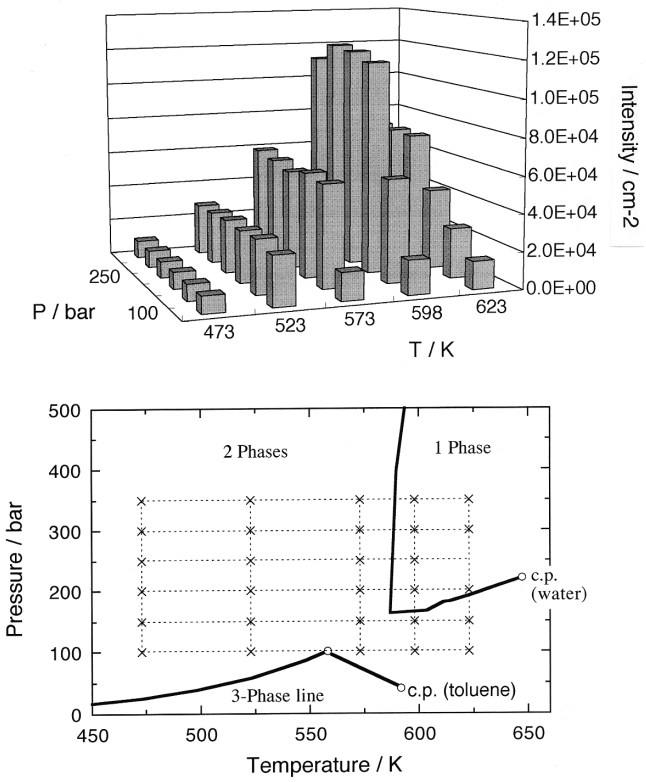


Fig. 16. Infrared intensity map for HDO in the toluene-rich phase (upper) and the typical experimental points indicated in the phase diagram (lower).

(lower). It is seen that all the experimental points at 473 and 523 K are in the two-phase region and are distinctly above the three-phase equilibrium line. Then the present experimental results indicate that the water concentration in the two-phase region increases remarkably by going left-to-right along a horizontal line in the phase diagram, but it changes little along a vertical line, at least in the 100–350 bar range. In contrast, at the higher temperatures, the water concentration remarkably increases along a vertical line.

Such temperature-pressure-dependency of water concentration is conveniently shown by a three-dimensional intensity map in Fig. 15 (upper). Similar intensity behavior has been found for the water–toluene and water–ethylbenzene mixtures, as shown in Fig. 16, but the temperature for the steepest increase shifts to somewhat higher temperatures, probably corresponding to shifts of the three-phase critical points.

These remarkable pressure dependences of the integrated intensities or the water concentrations should be characteristic of fluid mixtures in a near critical region. It is well known that the density of a pure substance exhibits a drastic but continuous pressure dependence at temperatures slightly above the gas–liquid critical temperature.[64] By analogy with this fact, the density of the water–aromatic hydrocarbons is expected to show remarkable pressure dependence at temperatures slightly above the three-phase critical temperature. Although the critical behavior of a mixture will be more complicated than that of a pure substance, the above-mentioned pressure dependence of the water concentration should be related to the density of the mixtures. Therefore, it is intriguing to examine the temperature-pressure dependence of the density of the hydrocarbon-rich phase.

## 4. Molar Concentrations and Density

In order to estimate the density of the hydrocarbon-rich phase, we need molar concentrations of water and hydrocarbon in this phase. The water concentration has been estimated by means of an empirical relationship between the peak frequency and the molar integrated intensity. To estimate the concentration of hydrocarbons, we have measured the near-infrared absorption assigned to a phenyl group.

**4.1. Molar Concentration of Water.** The molar concentration of water, $C_w$, can be obtained from the integrated intensity of the OH stretching band, $A_{OH}$, divided by the molar absorption intensity, $A^m$,

$$C_w = A_{OH}/A^m. \tag{15}$$

We have proposed an empirical expression for the molar absorption intensity $A^m$ by allowing for an internal-field effect and effect of hydrogen-bond formation.[45] The results are as follows:

$$A^m = A_0{}^m/\Theta \tag{16}$$

$$\Theta = \frac{9n}{(n^2+2)^2} \tag{17}$$

$$A_0{}^m/(10^6\ \mathrm{cm\ mol^{-1}}) = 3.0 + 5.37 \times 10^{-2}\,(3707 - \nu_0/\mathrm{cm^{-1}}) + 2.12 \times 10^{-4}\,(3707 - \nu_0/\mathrm{cm^{-1}})^2 \tag{18}$$

where $\Theta$ denotes the internal-field correction factor given by the refractive index $n$ of the fluid mixture, and $A_0^m$ is the molar absorption intensity as a function of the band center frequency, $\nu_0$. The $n$ values can be estimated from the density of the mixture and the molar refraction of water and hydrocarbons. Using literature values of the mixture densities at some temperature–pressure points[2,32] and assuming additivity of the molar refraction,[65] we have estimated the values of the internal-field correction factor, $\Theta$, to be in the 0.82–0.90 range for the present experimental condition.[45] This rather narrow variation range of $\Theta$ indicates that the internal-field correction does not affect the similarity in the temperature–pressure dependence between the infrared integrated intensity and the water concentration. The expression of $A_0^m$, has been derived as an empirical relationship between the integrated intensities and the peak frequencies, both of which vary significantly by hydrogen bonding. As the hydrogen bond strengthens, the band center shifts to the lower frequency and the band intensity increases.[66] Taking account of this fact, we have obtained Eq. 18 using the molar absorption intensities and the peak frequencies of HDO in the gas, liquid and solid phases.[45] Since the observed bands are not symmetric and exhibit some structure, we have used the first moment of the absorption as the band center, $\nu_0$.

The resulting molar concentrations of water in the hydrocarbon-rich phase are plotted against temperatures at some pressures in Fig. 17. For the water–toluene and water–ethylbenzene mixtures, the $\Theta$ values have been approximated by those for the water–benzene mixture. It is obvious that, with increasing temperature at constant pressure, the water concentration reaches the maximum at a certain temperature and then steeply decreases at higher temperatures. Intriguingly, the positions of the turning points are close to the extended line of the three-phase equilibrium curve and/or the one-phase critical curve.

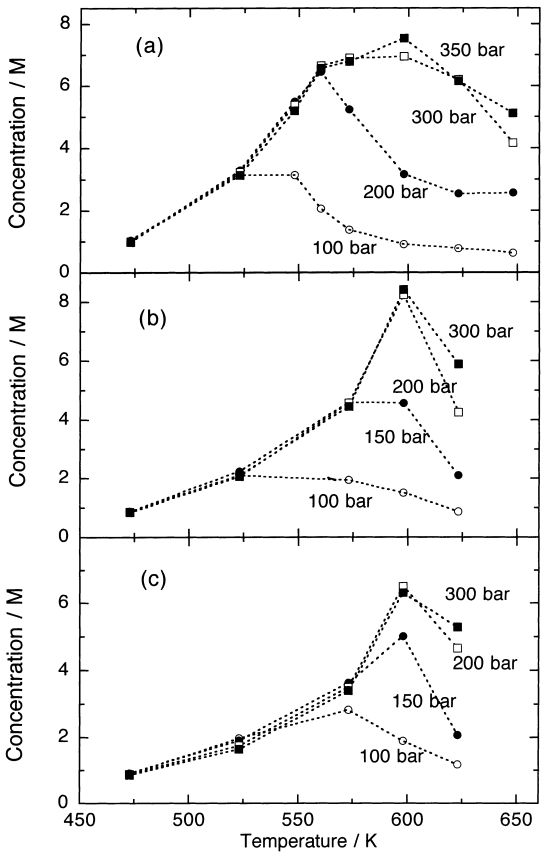


Fig. 17. Plots of water concentrations in benzene (a), toluene (b), and ethylbenzene (c) against temperature at some pressures.

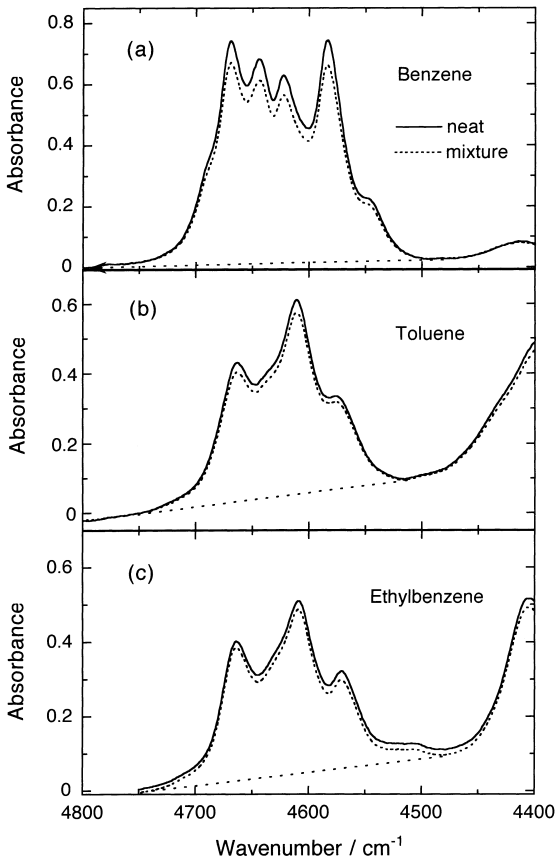


Fig. 18. Infrared absorption of benzene (a), toluene (b), and ethylbenzene (c) at 473 K and 100 bar. Solid line: neat liquid; dotted line: water-saturated liquid.

We should here take notice of the propriety of the present estimate of the water concentrations. It is based on rather crude approximations and has much room for improvement. Nevertheless, the water concentrations in benzene are approximately consistent with the previously reported values for limited ranges of temperature and pressure.[41,45] The uncertainty of the present estimates may be in the range of 10% to 20%.

**4.2. Concentration of Hydrocarbons in the Hydrocarbon-Rich Phase.** Figure 18 shows observed spectra of neat hydrocarbons and the hydrocarbon-rich phases of the water–hydrocarbon mixtures at 473 K and 100 bar. We deal with the absorption in the 4470–4800 $cm^{-1}$ range, which is assigned to a few combination transitions of the phenyl groups.[67] The molar absorption intensities of neat hydrocarbons, $A_{neat}^m$, are estimated from the integrated intensities, $S_{neat}$, in the spectral ranges 4470–4800 $cm^{-1}$ for benzene, 4520–4750 $cm^{-1}$ for toluene, and 4480–4750 $cm^{-1}$ for ethylbenzene, as

$$A^{m}_{neat} = S_{neat}/(C^{0}_{H}\cdot l) \quad (19)$$

where $l$ is the sample thickness, and $C^{0}_{H}$ denotes the molar concentration of neat hydrocarbons and is estimated from literature data of the densities.[68–70] The resulting molar absorption intensities are almost independent of temperature and pressure, as shown in Fig. 19 for benzene, and we assume constant values: $(2.15 \pm 0.05) \times 10^5$ cm mol$^{-1}$ for benzene, $(1.69 \pm 0.10) \times 10^5$ cm mol$^{-1}$ for toluene, and $(1.77 \pm 0.15) \times 10^5$ cm mol$^{-1}$ for ethylbenzene. The value for benzene is consistent with the previously reported molar absorption intensity of $2.19 \times 10^5$ estimated in the 4493–4763 cm$^{-1}$ range at 298 K and 1 bar.[71]

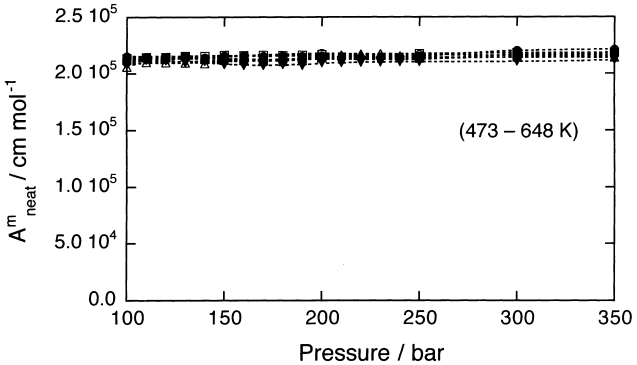


Fig. 19. Molar absorption intensities of neat benzene in the temperature–pressure range of 473–648 K and 100–350 bar.

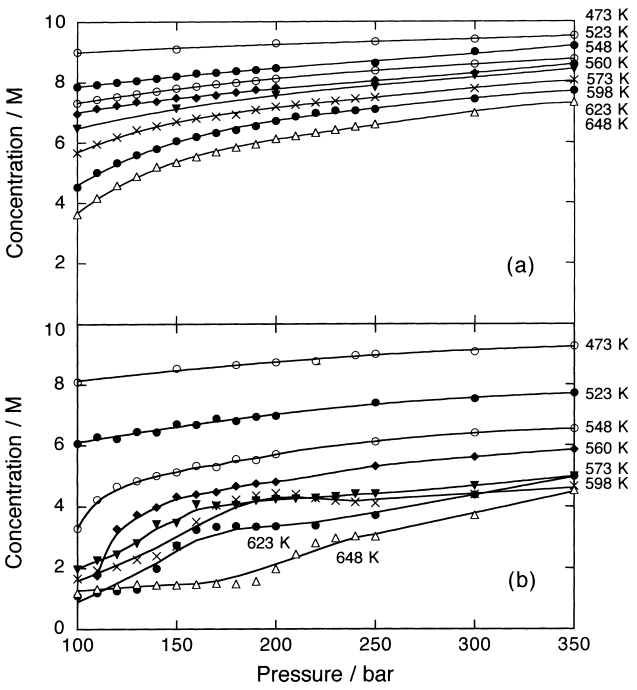


Fig. 20. Molar concentration of benzene in the neat fluid and in the water-saturated fluid plotted against pressure at various temperatures.

The molar concentration of the hydrocarbon in the hydrocarbon-rich phase, $C_H$, is estimated from the integrated intensity of the mixture, $S_{mix}$, by

$$C_H = S_{mix}/(A^{m}_{neat}\cdot l) \quad (20)$$

assuming that the molar absorption intensity in the mixture is the same as that in the neat hydrocarbons. This assumption is supported by the fact that the both spectra in that region are almost the same in profile and peak position, as seen in Fig. 18. The resulting molar concentrations for neat benzene and the water–benzene mixture are plotted against pressure in Fig. 20. Rather unusual fluctuations for the mixture at the higer temperatures and lower pressures are probably due to a slight temperature gradient in the cell, which may perturb the mixing state of the fluid particularly at the lower pressures. The concentration of benzene gradually increases with increasing pressure at constant temperature and decreases with increasing temperature at constant pressure. Obviously, the concentration of benzene in the benzene-rich phase of the mixture is lower than that of neat benzene. Needless to say, dissolution of water into the benzene-rich phase give rise to the decrement of the benzene concentration.

**4.3. Ratio of the Water Concentration and the Density.** Using the results of the water and hydrocarbon concentrations, we estimate densities of the hydrocarbon-rich phase in the two-phase region and the homogeneous phase by

$$\rho_{mix} = C_W M_W + C_H M_H \quad (21)$$

where $M_W$ and $M_H$ denote the molecular weight of water and hydrocarbon, respectively. Figure 21 shows the ratio of the water concentration and the density, $C_W/\rho_{mix}$, plotted against pressure. Intriguingly enough, the ratios at 548 and 560 K show far milder pressure dependence as compared with the remarkable pressure dependence of water concentration seen in Figs. 14 and 17. This fact means that the density of the benzene-rich phase increases steeply with increasing pressure in about the same way as that for the water concentration. In addition, the ratios slightly decrease with increasing pressure in the temperature range 473–560 K, which is lower than the crit-

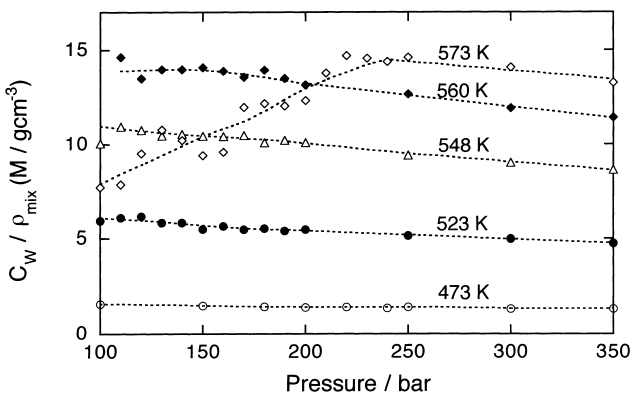


Fig. 21. Plots of ratio of the water concentration to the density of the benzene-rich phase against pressure at some temperatures.

ical solution temperature, 567 K,[4] the lowest temperature in the critical curve. A similar tendency has been observed for the water–toluene and water–ethylbenzene mixtures.

At 573 K, on the contrary, the ratio increases initially and then seems to become constant or slightly decrease at higher pressures. In other words, as the pressure goes up along the vertical line in the phase diagram shown in Fig. 15, the water concentration increases somewhat faster than the density up to around the crossing point over the critical curve. A similar tendency has been found at the higher temperatures, although the calculated values suffered from large uncertainty. To discuss this phenomenon further, the uncertainty of the experimental data at higher temperatures and lower pressures must be significantly reduced.

Observation of the above-mentioned phenomena has become possible for the first time by the in situ spectroscopic measurements. The present results are the first measurements of the temperature-pressure-dependent change of the density of the one phase in a two-phase coexistence region of the fluid mixtures, to our knowledge.

## 5. Conclusion

It has been shown that in situ infrared measurements contain various types of useful information about the water–hydrocarbon mixtures at high temperatures and pressures. Infrared absorption of HDO in aromatic hydrocarbons measured as a function of temperature and pressure has been analyzed. At temperatures lower than the three-phase critical end point, the absorption can be decomposed into the hydrogen-bond-free and hydrogen-bonded bands. The intensity ratio of the latter to the former increases with increasing temperature against the unfavorable entropy effect. This is explained by a high enough increasing rate of water solubility with increasing temperature. A good correlation is found between the OH stretching frequency and the ionization potential of the solvent hydrocarbons. Then, it is indicated that the concept of the $\pi$-hydrogen bonding, which has been proposed for a water–benzene complex at extremely low temperatures, is still useful for understanding water–hydrocarbon interaction even at high temperatures and pressures. The significant temperature-dependent change in the band profile suggests that a water molecule rotates rather freely even in a hydrogen-bonded water cluster at high enough temperatures. At temperatures higher than the three-phase critical end point, the absorption intensity as a measure of water concentration increases remarkably with increasing pressure, particularly around the extended line of the three-phase coexistence curve. This is found to be parallel to pressure dependent-change in the density of the hydrocarbon-rich phase. The steep continuous increase in the density in the region near the three-phase critical end point resembles well-known observations for pure fluids near the critical point, and should be characteristic of fluid mixtures near the critical region. This phenomenon is observed for the first time by the present in situ infrared measurements.

This work was supported by the Research Fellowships of the Japan Society for the Promotion of Science for Young Scientist to S.F.

## References

1 C. J. Rebert and W. B. Kay, *AIChE J.*, **5**, 285 (1959).
2 W. H. Thompson and J. R. Snyder, *J. Chem. Eng. Data*, **9**, 516 (1964).
3 J. F. Connolly, *J. Chem. Eng. Data*, **11**, 13 (1966).
4 Z. Alwani and G. M. Schneider, *Ber. Bunsen-Ges. Phys. Chem.*, **71**, 633 (1967).
5 G. A. Jeffrey and W. Saenger, "Hydrogen Bonding in Biological Structures," Springer-Verlag, Berlin (1991).
6 T. Lazaridis, G. Archontis, and M. Karplus, *Adv. Protein Chem.*, **47**, 231 (1995).
7 G. I. Makhatadze and P. L. Privalov, *Adv. Protein Chem.*, **47**, 307 (1995).
8 J. Peng and A. Wan, *Environ. Sci. Technol*, **31**, 2998 (1997).
9 C. M. Stellman, K. J. Ewing, F. Bucholtz, and I. D. Aggarwal, *Sens. Actuators, B*, **53**, 173 (1998).
10 J. S. Rowlinson and F. L. Swinton, "Liquids and Liquid Mixtures," 3rd ed, Butterworth, London (1982).
11 C. Tsonopoulos and G. M. Wilson, *AIChE J.*, **29**, 990 (1983).
12 C. J. Wormald, *Ber. Bunsen-Ges. Phys. Chem.*, **88**, 826 (1984).
13 J. Li, I. Vanderbeken, S. Ye, H. Carrier, and P. Xans, *Fluid Phase Equilibria*, **131**, 107 (1997).
14 Th. Hirth and E. U. Franck, *Ber. Bunsen-Ges. Phys. Chem.*, **97**, 1091 (1993).
15 I. Hua, R. H. Hochemer, and M. R. Hoffmann, *J. Phys. Chem.*, **99**, 2335 (1995).
16 T. Sako, T. Sugeta, K. Otake, M. Sato, M. Tsugumi, T. Hiaki, and M. Hongo, *J. Chem. Eng. Jpn.*, **30**, 744 (1997).
17 W. C. Bell, K. S. Booksh, and M. L. Myrick, *Anal. Chem.*, **70**, 332 (1998).
18 Y. Yamasaki, H. Enomoto, N. Yamasaki, and M. Nakahara, *Bull. Chem. Soc. Jpn.*, **73**, 2687 (2000).
19 J. L. DiNaro, J. W. Tester, J. B. Howard, and K. C. Swallow, *AIChE J.*, **46**, 2274 (2000).
20 E. U. Franck, *Ber. Bunsen-Ges. Phys. Chem.*, **88**, 820 (1984).
21 C. J. Wormald, N. M. Lancaster, and C. J. Sowden, *J. Chem. Soc., Faraday Trans.*, **93**, 1921 (1997).
22 I. M. Abdulagatov, A. R. Bazaev, E. A. Bazaev, M. B. Saidakhmedova, and A. E. Ramazanova, *J. Chem. Eng. Data*, **43**, 451 (1998).
23 J. G. Roof, *J. Chem. Eng. Data*, **15**, 301 (1970).
24 Th. W. De Loos, W. G. Penders, and R. N. Lichtenthaler, *J. Chem. Thermodyn.*, **14**, 83 (1982).
25 J. L. Heidman, C. Tsonopoulos, C. J. Brady, and G. M. Wilson, *AIChE J.*, **31**, 376 (1985).
26 I. G. Economou, J. L. Heidman, C. Tsonopoulos, and G. M. Wilson, *AIChE J.*, **43**, 535 (1997).
27 E. Brunner, *J. Chem. Thermodyn.*, **22**, 335 (1990).
28 T. Yiling, Th. Michelberger, and E. U. Franck, *J. Chem. Thermodyn.*, **23**, 105 (1991).
29 M. Meichel and E. U. Franck, *J. Supercrit. Fluids*, **9**, 69 (1996).
30 R. C. Reid, J. M. Prausnitz, and T. K. Sherwood, "The Properties of Gases and Liquids," 3rd ed, McGraw Hill, New York (1977).
31 P. H. van Konynenburg and R. L. Scott, *Philos. Trans. R. Soc. London, A*, **298**, 495 (1980).

32 R. Deul and E. U. Franck, *Ber. Bunsen-Ges. Phys. Chem.*, **95**, 847 (1991).
33 K. Chandler, B. Eason, C. L. Liotta, and C. A. Eckert, *Ind. Eng, Chem. Res.*, **37**, 3515 (1998).
34 Von E. Greinacher, W. Lüttke, and R. Mecke, *Z. Elektochem.*, **59**, 23 (1955).
35 L. B. Magnusson, *J. Phys. Chem.*, **74**, 4221 (1970).
36 T. A. Shippey, M. C. R. Symons, and J. A. Brivati, *Mol. Phys.*, **38**, 1693 (1979).
37 S. Yamazaki, S. Ikawa, and M. Kimura, *J. Quant. Spectrosc. Radiat. Transfer*, **24**, 421 (1980).
38 T. Tassaing, M. Besnard, Y. Danten, E. Zoidis, J. Yarwood, Y. Guissani, and B. Guillot, *Mol. Phys.*, **84**, 769 (1995).
39 M. Besnard, Y. Danten, and T. Tassaing, *J. Chem. Phys.*, **113**, 3741 (2000).
40 J. A. B. Ferreira, L. M. Ilharco, and S. M. B. Costa, *Spectrochim. Acta A*, **57**, 137 (2001).
41 T. Tassaing, *Vib. Spectrosc.*, **24**, 15 (2000).
42 J. Pironon, R. Thiéry, S. Teinturier, and F. Walgenwitz, *J. Geochem. Explor.*, **69-70**, 663 (2000).
43 S. Furutaka and S. Ikawa, *J. Chem. Phys.*, **108**, 1347 (1998).
44 S. Furutaka and S. Ikawa, *J. Chem. Phys.*, **108**, 5159 (1998).
45 S. Furutaka and S. Ikawa, *J. Chem. Phys.*, **113**, 1942, 8390 (E) (2000).
46 S. Furutaka and S. Ikawa, *Fluid Phase Equilib.*, in press.
47 T. C. Poulter, *Phys. Rev.*, **40**, 860 (1932).
48 R. A. Toth and J. W. Brault, *Appl. Opt.*, **22**, 908 (1983).
49 J. G. C. M. van Duijneveldt-van de Rijdt and F. B. van Duijneveldt, *Chem. Phys.*, **175**, 271 (1993).
50 D. Forney, M. E. Jacox, and W. E. Thompson, *J. Mol. Spectrosc.*, **157**, 479 (1993).
51 G. P. Ayers and A. D. E. Pullin, *Spectrochim. Acta*, A, **32**, 1629 (1976).
52 L. Fredin, B. Nelander, and G. Ribbegard, *J. Chem. Phys.*, **66**, 4065 (1977).
53 R. M. Bentwood, A. J. Barnes, and W. J. Orville-Thomas, *J. Mol. Spectrosc.*, **84**, 391 (1980).
54 C. J. Gruenloch, J. R. Carney, C. A. Arrington, T. S. Zwier, S. Y. Fredericks, and K. D. Jordan, *Science*, **276**, 1678 (1997).
55 A. Engdahl and B. Nelander, *J. Phys. Chem.*, **91**, 2253 (1987).
56 S. Suzuki, P. G. Green, R. E. Bumgarner, S. Dasgupta, W. A. Goddard III, and G.A. Blake, *Science*, **257**, 942 (1992).
57 H. Ratajczak and W. J. Orville-Thomas, *J. Mol. Struct.*, **19**, 237 (1973).
58 R. S. Mulliken, *J. Am. Chem. Soc.*, **74**, 811 (1952).
59 S. Furutaka and S. Ikawa, unpublished data.
60 R. S. Mulliken and W. B. Person, "Molecular Complexes," John Wiley & Son, New York (1969).
61 W. J. Griffiths and F. M. Harris, *Org. Mass. Spectrom.*, **22**, 559 (1987).
62 S. Y. Fredericks, K. D. Jordan, and T. S. Zwier, *J. Phys. Chem.*, **100**, 7810 (1996).
63 O. Matsuoka, E. Clementi, and M. Yoshimine, *J. Chem. Phys.*, **64**, 1351 (1976).
64 E. A. Guggenheim, "Thermodynamics," North-Holland, Amsterdam (1967).
65 C. J. F. Bottcher, "Theory of Electric Polarization," Elsevier, Amsterdam (1952).
66 G. C. Pimentel and A. L. McClellan, "The Hydrogen Bond," Freeman, SanFrancisco (1960).
67 M. Causse and P. Barchewitz, *J. Physique Rad. Ser. 8*, **10**, 49 (1949).
68 R. D. Goodwin, *J. Phys. Chem. Ref. Data*, **17**, 1541 (1988).
69 T. S. Akhundov, *Izv. Vyssh. Uchebn. Zaved. Neft Gaz*, **11**, 20, 112 (1973).
70 A. Pruss and W. Wagner, In NIST Chemistry WebBook-Thermophysical Properties of Fluid Systems (NIST Standard Reference Database No. 69, The National Institute of Standards and Technology, 1998). http://webbook.nist.gov /chemistry/fluid/
71 J. E. Bertie, R. N. Jones, and C. D. Keefe, *Appl. Spectrosc.*, **47**, 891 (1993).

Seiya Furutaka was born in 1972 in Chiba, Japan. He graduated from Yokohama National University (1996), where he performed the structural study of supercritical $CO_2$ by X-ray diffraction under the direction of Prof. Keiko Nishikawa. In 1996 he started as a graduate student in Hokkaido University under the supervision of Prof. Shun-ichi Ikawa. From 1999 to 2001, he was a JSPS Research Fellow (DC). In 2001 he received his Ph.D. with the thesis entitled "Infrared Spectroscopic Study of Water–Hydrocarbon Mixtures at High Temperatures and Pressures". He is currently a JSPS Research Fellow (PD). His research interest is in the molecular level mechanism of the effect of the salt on the phase behavior of the water–hydrocarbon mixtures at high temperatures and pressures.

Hitomi Kondo was born in 1975 in Nara, Japan. She graduated from Hokkaido University in 1999 with B.S. degree in chemistry. In 2001 she received her M.S. degree in chemistry from Hokkaido University, where she was engaged in the infrared study of water–toluene and water–ethylbenzene mixture at high temperatures and pressures. She is now working at Nippon Information and Communication Corp. (NI + C).

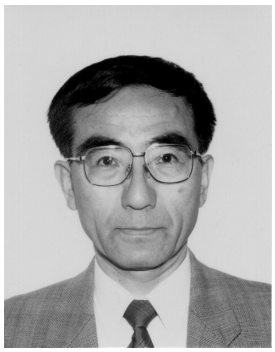

Shun-ichi Ikawa was born in Tokyo and educated at Tokyo Institute of Technology where he obtained his B.S. (1964), M.S. (1966) and D.S. degrees (1969) in chemistry. In 1969, he joined Hokkaido University, and currently has a position of Professor in Division of Chemistry, Graduate School of Science. His research interest is in structure and dynamics of molecules in the liquid phase and in supercritical fluids. He has been engaged in high-pressure spectroscopy since 1981 when he worked at NRC Canada as a research associate (1981–1983) under the supervision of the late Dr. Whalley. He is currently conducting spectroscopic study of supercritical fluid mixtures in the vicinity of the critical region.